23rd ABCM International Congress of Mechanical Engineering
December 6-11, 2015, Rio de Janeiro, RJ, Brazil

# COMPARISON OF ACTIVE THERMOGRAPHY TECHNIQUES FOR THE INSPECTION AND DEFECT CHARACTERISATION OF CARBON FIBER COMPOSITES

**Henrique Coelho Fernandes**
Computer Vision and Systems Laboratory, Laval University, Quebec City (Quebec) G1K 7P4, Canada
Henrique-Coelho.Fernandes.1@ulaval.ca

**Marc Georges**
**Georges Crabus**
Centre Spatial de Liège - Université de Liège, Liege Science Park, Avenue du Pré Aily, 4031 Angleur (Liège) - Belgium
mgeorges@ulg.ac.be, c_g_steph@hotmail.com

**Clemente Ibarra-Castanedo**
**Xavier Maldague**
Computer Vision and Systems Laboratory, Laval University, Quebec City (Quebec) G1K 7P4, Canada
{IbarraC, Xavier.Maldague}@gel.ulaval.ca

***Abstract.*** *Active thermography is a nondestructive testing (NDT) technique that has been gaining popularity in the aerospace industry, among several other fields. It has been proposed as an valuable alternative to well-known NDT methods such as radiography and ultrasound testing for the assessment of composites materials given its relatively ease of implementation, i.e. it is fast and allows the inspection of large surfaces in situ, at once and without the need of disassembling any component. In this work, different active thermography techniques (pulsed thermography, vibrothermography and line scan thermography) are examined in order to inspect carbon fiber academic samples with artificial defects (flat-bottom-holes). Different processing techniques are presented and they are compared based on signal-to-noise calculations for defect detectability. A quantitative approach for depth retrieval with pulsed thermographic data is presented as well.*

***Keywords:*** *active thermography, pulsed thermography, vibrothermography, line scan thermography, carbon fiber composites*

## 1. INTRODUCTION

Composite materials (CM) in transport aircraft components are being used for decades. Prior to the mid-1980s, aircraft manufacturers used CM in transport category aircraft in secondary structures (e.g., wing edges) and control surfaces. In 1988, Airbus introduced the A320, the first aircraft in production with an all-composite tail section and, in 1995, the Boeing Company introduced the Boeing 777, also with a composite tail section. CM used in commercial aircraft typically are produced by combining layers of carbon or glass fibers with epoxy.

In recent years, manufacturers have expanded the use of composites to the fuselage and wings because these materials are typically lighter and more resistant to corrosion than are the metallic materials that have traditionally been used in aircraft. Nevertheless, their strength and stiffness are comparable to metals. The Boeing 787 is the first mostly composite large transport aircraft in commercial service. The Boeing 787 weight is about 50% composite (excluding the engines) as reported by Hale (2006). It carries 210-330 passengers.

This increasing demand motivates the industry to not only develop better and more cost efficient technique to manufacture these materials but also to develop techniques to inspect and assure the quality of these materials during their life time. Infrared Thermography (IT) is a widely used nondestructive testing (NDT) technique for diagnostics and motoring in several areas including composite materials. Some of the reasons for its popularity are that it is a safe technique, usually contactless and has a fast inspection rate that allows the inspection of large surfaces in situ at once and without the need of disassembling any component. According to Maldague (2001), in active IT an external heat source is used to stimulate the material being inspected in order to generate a thermal contrast between the feature of interest and the background. The active approach is adopted in many cases given that the inspected parts are usually in equilibrium with the surroundings.

In this paper, different active thermography techniques (pulsed thermography, vibrothermography and line scan thermography) are examined in order to inspect carbon fiber academic samples with artificial defects (flat-bottom-holes). The advantages of each of these techniques are discussed and compared based on signal-to-noise calculations for defect detectability. A quantitative approach for depth retrieval with pulsed thermographic data is presented as well.

## 2. MATERIAL AND METHODS

### 2.1 Inspected samples

The sample inspected in this paper is a carbon fiber reinforced polymer (CFRP) plate. It has six artificial defects manufactured for academic purposes. The defects are flat-bottom-holes (FBH) at three different depths and with two different diameters. CFRP01 is 2.2 mm thick and 148.5 mm x 185 mm of length and width. Figure 1a shows the position of each defect while Figure 1b show the depth and diameter of the defects. Thermal diffusivity ($\alpha$) of CFRP adopted that is used latter for the quantification of the depth using the phase is $4.2 * 10^{-7} \left(m^2/s\right)$.

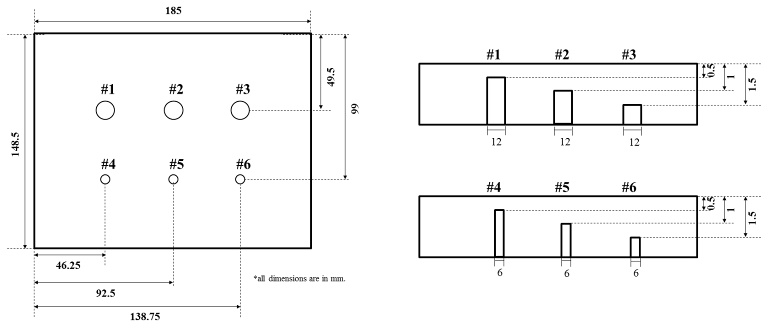


(a) (b)

Figure 1: Inspected CFRP plate and position, diameter and depth of each defect.

### 2.2 Pulsed Thermography (PT)

In pulsed thermography (PT), the specimen surface is submitted to a heat pulse using a high power source such as photographic flashes. A heat pulse can be considered as the combination of several periodic waves at different frequencies and amplitudes. After the thermal front comes into contact with the specimen's surface, heat travels from the surface through the interior of the specimen by conduction. As time elapses, the surface temperature will decrease uniformly for a piece without internal flaws. On the contrary, subsurface discontinuities (e.g. porosity, delaminations, disbonds, fiber breakage, inclusions, etc.), can be seen as resistances to heat flow that produce abnormal temperature patterns at the surface, which can be detected with an IR camera.

Data acquisition in PT is fast and straightforward as illustrated in Figure 2. Flashes can be used to heat up the specimen's surface, and subsequently, the thermal changes are recorded with an infrared camera. Data is stored as a 3D matrix (Figure 3a) where $x$ and $y$ are the spatial coordinates, and $t$ is the time. Temperature decreases approximately as $t^{1/2}$ (at least at early times) for a sound area. However, the cooling rate of a defective zone is different from a sound area. An example of temperature profiles of a sound area and a defective zone are showed in Figure 3b. These defective zones appear sometimes as subtle signatures in the infrared images. Thus, image processing techniques are needed in order to enhance the quality of the images and enable the qualitative and quantitative assessment of the inspected plate. The techniques used in this work to enhance the infrared images are presented in section 2.5

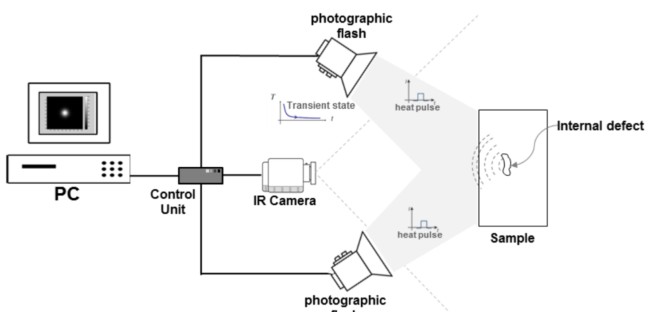


Figure 2: Possible set-up for a PT inspection. Adapted from Ibarra-Castanedo and Maldague (2013)

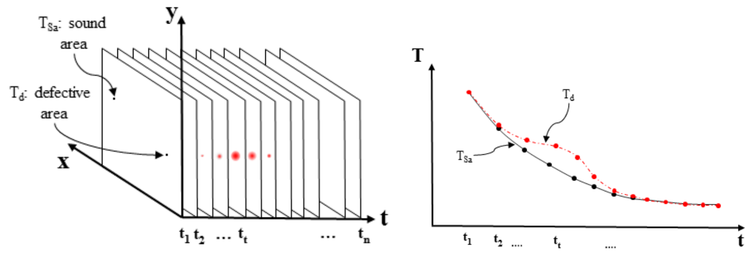


(a) (b)

Figure 3: Temperature evolution. (a) data 3D matrix. (b) temperature profiles of defective and sound areas.

### 2.3 Line Scan Thermography (LST)

Line scan thermography (LST) is a dynamic active thermography technique, which can be employed for the inspection of materials by heating a component, line-by-line, while acquiring a series of thermograms with an infrared camera. This can be done in two ways, either the thermographic head as described by Woolard and Cramer (2005), consisting of an infrared camera and an energy source, moves along the surface while the part is motionless or, as in Oswald-Tranta and Shepard (2013), it may be the component that is in motion while the thermographic head stands still. In both cases, the thermal history for every pixel or line of pixels can be precisely tracked by controlling the heating source speed and the rate of data acquisition. In the original acquisition sequence the inspected sample appears to be moving so the sequence must be reconstructed in order to have the variation on time and not on space. The reconstructed matrix is obtained by following the temporal evolution of every pixel line independently, in such a way that, a given pixel line of the original sequence is recovered frame by frame (through time) and reallocated into a new sequence of images. Figure 4 shows a possible set-up for a LST inspection. In Figure 4 the thermographic head is composed by the a infrared camera and a heat source (an electrical actuator with a quartz infrared lamp of 1600W). The thermographic head moves in one sense (top to bottom) covering the entire surface of the sample to be inspected while the last remains motionless.

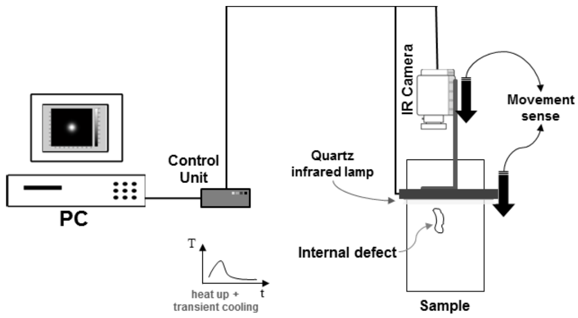


Figure 4: Line Scan Thermography schematic set-up.

### 2.4 Vibrothermography (VT)

In contrast to the two first approaches where the energy is delivered to the sample externally, in vibrothermography the energy is generated internally. Vibrothermography (VT), also known as ultrasound thermography (Shepard *et al.*, 2004), utilizes mechanical waves to directly stimulate internal defects and without heating the surface as in optical methods. In VT, ultrasonic waves will travel freely through a homogeneous material, whereas an internal defect will produce a complex combination of absorption, scattering, beam spreading and dispersion of the waves, whose principal manifestation will be in the form of heat. Heat will then travel by conduction in all directions and an IR camera can be directed to one of the surfaces of the specimen to capture the defect signature. Ultrasonic waves are ideal for NDT since they are not audible to humans (although some low frequency harmonics are present), defect detection is independent from its orientation inside the specimen, and both internal and open surface defects can be detected. Hence, VT is very useful for the detection of cracks and delaminations. Figure 5 shows a schematic setup of a vibrothermography experiment where, similar to PT, an ultrasound wave burst is injected into the specimen (flash pulse in the PT case) and the temperature profiles are recorded with an infrared camera.

The ultrasound wave is produced by a transducer composed of a stack of piezo elements and concentrated in a titanium horn that acts like a hammer. Hence, the part being inspected should be firmly immobilized (but without damaging it) to avoid cantilever effects, clapping and sliding of the transducer. The transducer horn should be pressed against the sample as well to improve the coupling transmission of the ultrasound into the specimen. A bad coupling implies a poor

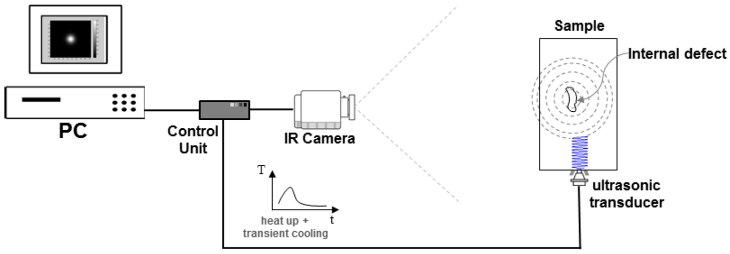


Figure 5: Vibrothermography schematic set-up. Adapted from Ibarra-Castanedo and Maldague (2013).

ultrasound transmission but more seriously it creates unwanted heat in the vicinity of the ultrasound injection point.

After the elastic waves are injected to the specimen, they travel through the material and dissipate their energy mostly at the defects generating frictional rubbing, thus heat is locally released (Mian *et al.*, 2004; Rothenfusser and Homma, 2005; Renshaw *et al.*, 2011). The thermal waves then travel by conduction to the surface where they can be detected with an IR camera.

When compared to optical/external techniques, the thermal wave travels half the distance in a VT experiment since heat propagation is performed from the defect to the surface, whereas for optical techniques heat travels from the surface to the defects and back to the surface. Thus, VT is very fast, even faster than PT. The duration of a typical experiment varies from a fraction of a second to several seconds. In addition, the longer the transducer operates at the surface, the more heat is released at the contact surface, increasing the probability of damaging the area. Furthermore, the pressure applied between the horn and the specimen has a great impact on the thermal response (Shepard *et al.*, 2004).

VT is extremely fast, although it is necessary to relocate the transducer (and to immobilize the specimen again) to cover a large area for inspection. Hence, VT is more suitable for relatively small objects. It is the most appropriate technique to inspect certain types of defects, e.g. micro cracks. On the contrary, it does not perform very well in some other cases in which application of optical techniques are straightforward, e.g. water detection. But probably the most inconvenient aspect of VT is the need to hold the specimen. On the other hand, there is only minimal heating of the inspected specimen since energy is usually dissipated mostly at the defective areas, although there is some localized heating at the coupling and clamping points.

### 2.5 Infrared Image Processing

#### 2.5.1 Principal Component Thermography (PCT)

Principal component thermography (PCT), originally proposed by Rajic (2002), extracts the image features and reduces the undesirable signals. It relies on singular value decomposition (SVD), which is a tool to extract spatial and temporal data from a matrix in a compact manner by projecting original data onto a system of orthogonal components known as empirical orthogonal functions (EOF). By sorting the principal components in such way that the first EOF represents the most characteristic variability of the data, the second EOF contains the second most important variability, and so on, the original data can be adequately represented with only a few EOFs.

The SVD of a $MxN$ matrix A, where $M > N$, can be calculated as follows:

$$A = URV^T \tag{1}$$

where $U$ is a $MxN$ orthogonal matrix, $R$ being a diagonal $NxN$ matrix (with singular values of $A$ present in the diagonal), $V^T$ is the transpose of a $NxN$ orthogonal matrix (characteristic time) as proposed in Rajic (2002).

Hence, in order to apply the SVD to thermographic data, the 3D thermogram matrix representing time and spatial variations has to be reorganised as a 2D $MxN$ matrix $A$. This can be done by rearranging the thermograms for every time as columns in $A$, in such a way that time variations will occur column-wise while spatial variations will occur row-wise. Under this configuration, the columns of $U$ represent a set of orthogonal statistical modes known as empirical orthogonal functions (EOF) that describe the data spatial variations. On the other hand, the principal components (PCs), which represent time variations, are arranged row-wise in matrix $V^T$. The first EOF will represent the most characteristic variability of the data; the second EOF will contain the second most important variability, and so on. Usually, original data can be adequately represented with only a few EOFs. Typically, an infrared sequence of 1000 images can be replaced by 10 or less EOFs.

#### 2.5.2 Thermographic Signal Reconstruction (TSR)

Thermographic signal reconstruction (TSR), proposed by Shepard (2001) and recently reviewed in Shepard and Beemer (2015), is an attractive technique that allows increasing the spatial and temporal resolution of a sequence, while reducing the amount of data to be manipulated. TSR is based on the assumption that temperature profiles for non-defective pixels should follow the decay curve given by the 1D solution of the Fourier equation which may be rewritten in the logarithmic form, as in Shepard (2001), as:

$$\ln(\Delta T) = \ln\left(\frac{Q}{e}\right) - \frac{1}{2}\ln(\pi t) \quad (2)$$

Nevertheless, the 1D solution of the Fourier equation is only an approximation. Shepard (2001) proposed to expand the logarithmic form into a series to fit the thermographic data. This is performed by using a $n$-degree polynomial of the form:

$$\ln(\Delta T) = a_0 + a_1\ln(t) + a_2\ln^2(t) + \cdots + a_n\ln^n(t) \quad (3)$$

The thermal profiles corresponding to non-defective areas in the sample will approximately follow a linear decay, while a defective area will diverge from this linear behaviour. At the end, the entire raw thermogram sequence is reduced to $n+1$ coefficient images (one per polynomial coefficient) from which synthetic thermograms can be reconstructed.

Synthetic data processing brings interesting advantages such as: significant noise reduction, possibility for analytical computations and data compression (from the original number of infrared images in the sequence to $n+1$ images). As well, analytical processing provides the possibility of estimating the actual temperature for a time between acquisitions from the polynomial coefficients. Furthermore, the calculation of first and second time derivatives from the synthetic coefficients is straightforward as showed in Shepard (2001). The first time-derivative indicates the rate of cooling while the second time-derivative refers to the rate of change in the rate of cooling. Therefore, time derivatives are more sensitive to temperature changes than raw thermal images.

### 2.5.3 Pulsed Phase Thermography (PPT)

In pulsed phase thermography (PPT), originally proposed by Maldague and Marinetti (1996) and recently reviewed by Ibarra-Castanedo and Maldague (2015), data is transformed from the time domain to the frequency spectra using the 1D discrete Fourier transform (DFT):

$$F_n = \Delta t \sum_{k=0}^{N-1} T(k\Delta t)exp^{(-j2\pi nk/N)} = Re_n + Im_n \quad (4)$$

where $j$ is the imaginary number, $n$ designates the frequency increment ($n = 0, 1, ...N$), $\Delta t$ is the sampling increment, and $Re$ and $Im$ are the real and imaginary parts of the transform respectively. In this case, real and imaginary parts of the complex transform are used to estimate the amplitude and the phase as described in Ibarra-Castanedo and Maldague (2004):

$$A_n = \sqrt{Re_n^2 + Im_n^2} \quad (5)$$

$$\phi_n = tan^{-1}\left(\frac{Im_n}{Re_n}\right) \quad (6)$$

DFT can be applied to any waveform. The phase, equation 6, is of particular interest in NDT&E given that it is less affected than raw thermal data by environmental reflections, emissivity variations, non-uniform heating, and surface geometry and orientation. These phase characteristics are very attractive not only for qualitative inspections but also for quantitative characterization of materials as will be pointed out latter.

As any other thermographic technique, PPT is not without drawbacks. The noise content is considerable, especially at high frequencies. A de-noising step is therefore often required. A combination of PPT and TSR is an interesting possibility, reducing noise and allowing the depth retrieval of defects as proposed in Ibarra-Castanedo (2005); Ibarra-Castanedo *et al.* (2005). A linear relationship exists between defect depth $z$ and the inverse square root of the blind frequency (which can be observed form experimental data). According to Bai and Wong (2001), blind frequency ($f_b$) is the frequency at which the phase contrast is enough for a defect to be visible (at frequencies higher than $f_b$, it is not possible to detect it). The thermal diffusion length ($\mu$), described by Busse and Rosencwaig (1980), can be used to fit experimental data and estimate the depth ($z$) as proposed by Ibarra-Castanedo (2005):

$$z = C_1\sqrt{\frac{\alpha}{\pi . f_b}} = C_1\mu \quad (7)$$

where the thermal diffusion length is $\mu = (2\alpha/\omega)$ [m], $\omega$ [rad/s] is the angular frequency, $\alpha$ is the thermal diffusivity of the material, $f_b$ [Hz] is the blind frequency and $C_1$ is an empirical constant where has been observed that $1.5 < C_1 < 2$ when working with the phase, with $C_1 = 1.82$ typically adopted in several worksz such as in Meola and Carlomagno (2004); Meola *et al.* (2004).

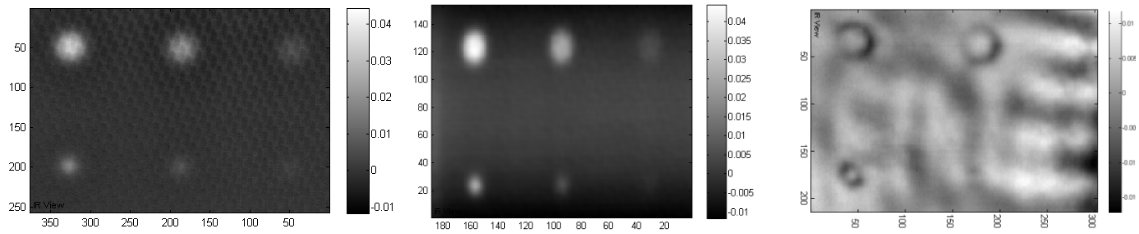

(a) (b) (c)

Figure 6: PCT results. (a) PT - 2nd EOF image, (b) LST - 1st EOF image and (c) VT - 3rd EOF image.

## 3. RESULTS AND DISCUSSION

Figure 6 shows qualitative results obtained with PCT of PT, LST and VT. Figure 6a shows the second EOF image obtained with PCT of a pulsed thermography inspection. It is possible to visualize a signature of all six defects. Despite of having a small contrast, even the small defect at 1.5 mm deep is detectable with PT. A similar result was obtained with the line scan thermography technique using 20 mm/s inspection speed. Figure 6b show the first EOF image obtained with this LST inspection. Figure 6c shows the third EOF image obtained with PCT of a vibrothermography inspection. The result reveals just the two defects at depth 0.5 mm and the largest defect (diameter: 12 mm) at depth 1 mm. The deepest defects were not detected (at 1.5 mm) nor the small defect (diameter: 6 mm). The weaker performance of VT when compared to optical techniques (PT and LST) is due the characteristic of the inspected defects: flat-bottom holes. The heat is mainly generated due to frictional rubbing near the defects and due to the nature of flat-bottom holes, heat is not generated enough near the defects and consequentially they are not detectable. On the other hand, VT performs very well detecting cracks.

A comparison of image processing techniques was also performed for Pulsed Thermography. First, TSR was applied on the raw thermal image after subtracting a cold image (an image before heating) to the whole sequence of thermograms, as proposed by Balageas (2012), in order to obtained smother profiles (7-degree polynomial was used). Then, using the fitted data, PCT, PPT, first and second derivatives images were calculated. Signal-to-noise ratio (SNR) was used to compare the results obtained. For each defect, a region inside the defect region was chosen as well as a near sound area region was arbitrary defined and then the SNR was calculated for each defect. Figure 7 shows the results obtained. Figure 7a and Figure 7e show the the second EOF image obtained with PCT and the plot of the profiles along the two line of defects. In Figure 7a, defect areas and respective sound areas for defects #1 and #4, which are 0.5 mm deep, are depicted in the image (images are fliped in relation to Figure 6 and Figure 1). Also, the white dotted line indicates the location of the lines that were plotted in Figure 7e. In a similar manner, Figure 7b and Figure 7f display the results obtained with the second phase image generated with PPT; Figure 7c and Figure 7g display the results obtained with the first derivative; and Figure 7d and Figure 7h show the results obtained with the second derivative. It is important to state that, for each of the techniques the best possible image was selected to perform the comparisons.

Table 1 shows the SNR values calculated for each defect using the different techniques for processing the sequence obtained with PT inspection. The larger the SNR value the better the defect is visualized in the image. In general, PCT

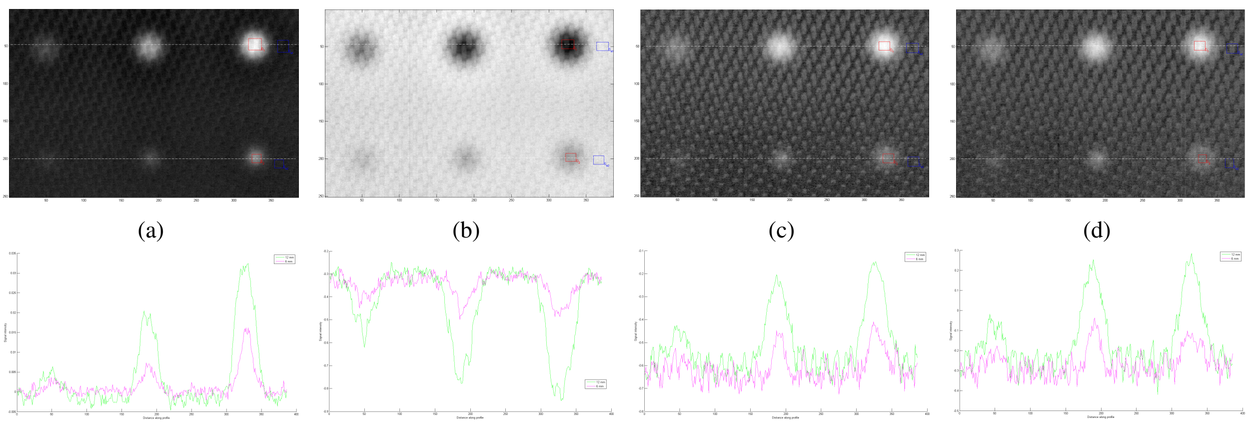

(a) (b) (c) (d)

(e) (f) (g) (h)

Figure 7: Comparison of different techniques applied on PT. First row shows the best image obtained with each technique and second row shows the profiles over each line of defects for the respective image. (a,e) PCT, (b,f) phase from PPT, (c,g) 1st derivative and (d,h) 2nd derivative.

Table 1: Signal-to-noise ratio of each defect for each processing technique.

| Defect # | Diameter[1] | Depth[1] | TSR+PCT | TSR+PPT (pha.) | 1st der. | 2nd der. |
|---|---|---|---|---|---|---|
| 1 | 12 | 0.5 | 29.3892 | 28.3348 | 19.5692 | 19.2143 |
| 2 | 12 | 1.0 | 24.0062 | 25.8299 | 15.3244 | 17.8124 |
| 3 | 12 | 1.5 | 14.1004 | 19.8404 | 9.0555 | 10.4062 |
| 4 | 6 | 0.5 | 24.2168 | 19.5385 | 11.2131 | 8.4717 |
| 5 | 6 | 1.0 | 17.2290 | 15.6497 | 11.1318 | 12.6898 |
| 6 | 6 | 1.5 | 7.0063 | 10.3294 | 6.7374 | 7.2052 |

(1) all dimension are in mm

applied after TSR displayed the best results. It should be mentioned that PCT and PPT performances are greatly enhanced by applying them to the synthetic (de-noised) data obtained by TSR. SNR values from these two techniques are lesser when applied to raw (noisy) data.

Comparison of SNR values of the best image obtained with PCT from PT (displayed in the fourth column of Table 1) and SNR values of the best image obtained also with PCT but from the LST inspection (#1: 44.1328, #2: 39.1117, #3: 16.0724, #4: 32.3513, #5: 15.3039 and #6: 7.6116) indicates that both techniques, i.e. PT and LST, produce similar results. SNR values for LST are slightly better due to the fact that the reconstruction processes applied on the original LST sequence reduced the spatial resolution of the image and smoothed the background as well as the defects. These two factors enhanced LST signal-to-noise ratio values. However, it can be seen by comparing Figure 6a and Figure 6b that PT and LST images are visually very similar in terms of defect detectability.

Depth estimation for the PT inspection was performed using Equation 7. First, the raw data was fitted using a polynomial of degree 7. Then, PPT was applied on the fitted sequence and blind frequencies ($f_b$) of each defect were calculated. The respective blind frequencies for the defects #1 and #4 (at depth 0.5 mm) are $f_{b1}$ = 0.5 Hz and $f_{b4}$ = 0.88 Hz, which give estimated depths of 0.93 mm and 0.7 mm, respectively. Based on the specifications provided in Figure 1, both defects should be at the same depth. However, defect #1 is deeper than defect #4 according to the depth estimated by the phase. Also, even in the fitted temperature data, i.e. before applying PPT, it is possible to see that defect #4 appears earlier than defect #1, which indicates that defect #1 is deeper. Based of this observations, it is reasonable to conclude that they are not at the nominal depth that was specified. This could be explained by the fact that defects were hand made and imprecisions may occur.

Depth estimation of the other defects was not performed because of the infrared sequence obtained from the PT inspection was not long enough. New experimental testing would be required in order to increase the acquisition temporal window, which would allow to estimate the depths for the deepest defects (1 mm and 1.5 mm). Even though a quantitative assessment was not performed for these defects, they were assessed qualitatively as it can be seen in Figure 6 and in Figure 7.

## 4. CONCLUSIONS

In this work three different active infrared thermography inspection techniques were presented: pulsed thermography, line scan thermography and vibrothermography. An academic CFRP sample with artificial defects (flat-bottom-holes) were inspected. It was possible to detect all defects with the first two techniques. However, only the defects at 0.5 mm and the biggest defect at 1 mm were detectable using VT. Additionally, both PT and LST showed similar qualitative results. It suggests that, for the cases where the use of PT is restricted, e.g. when on is inspecting complex shaped parts, the use of LST is a viable solution. In this case the thermographic head would move in a controlled fashion (being able to move in all dimensions), for instance using a robot as proposed by Ibarra-Castanedo *et al.* (2014), in order to follow the shape of the sample.

Different data processing techniques were applied for PT: TSR, PCT and PPT. First, the sequence was processed by TSR where a 7 degree polynomial was used to fit the data reducing the influence of noise. Then, PCT and PPT were applied and also we calculated the 1st and 2nd derivative images from the fitted sequence. In order to compare the results, signal-to-noise ratios were calculated for each defect. PCT was the technique that better performed since it presented the largest SNR values. Finally, a depth estimation based on the phase was performed for defects at depth 0.5 mm. The estimated depth was different from the one specified, i.e. 0.5 mm. Additionally, the smaller defect (#4) is deeper than the larger defect (#1). Their estimated depths were 0.7 mm and 0.93 mm respectively while their nominal depth was 0.5 mm.

## 5. ACKNOWLEDGEMENTS

The authors would like to gratefully acknowledge support provided by the Canada Research Chair in Multipolar Infrared Vision (MiViM) and the Centre Spatial de Liège. Marc Georges would like to thank Wallonia SKYWIN project

ECOTAC (contract Nr 6490) and the Federation Wallonie-Bruxelles for supporting travels. The authors would also like to acknowledge the support of the following agencies: CNPq, National Council for Scientific and Technological Development - Brazil; NSERC, Natural Sciences and Engineering Research Council of Canada; FQRNT, Quebec Fund for Research on Nature and Technology.

## 6. REFERENCES

Bai, W. and Wong, B.S., 2001. "Evaluation of defects in composite plates under convective environments using lock-in thermography". *Measurement Science and Technology*, Vol. 12, No. 2, pp. 142–150.

Balageas, D.L., 2012. "Defense and illustration of time-resolved pulsed thermography for nde". *Quantitative InfraRed Thermography Journal*, Vol. 9, No. 1, pp. 3–32. doi:10.1080/17686733.2012.676902.

Busse, G. and Rosencwaig, A., 1980. "Subsurface imaging with photoacoustics". *Applied Physics Letters*, Vol. 36, No. 10, pp. 815–816.

Hale, J., 2006. "Boeing 787, from the ground up". *Aero Magazine*, Vol. 24, No. 4, pp. 16–23.

Ibarra-Castanedo, C., 2005. *Quantitative subsurface defect evaluation by pulsed phase thermography: depth retrieval with the phase.* Ph.D. thesis, Laval University, Canada.

Ibarra-Castanedo, C., Avdelidis, N.P. and Maldague, X., 2005. "Qualitative and quantitative assessment of steel plates using pulsed phase thermography". *Materials evaluation*, Vol. 63, No. 11, pp. 1128–1133.

Ibarra-Castanedo, C. and Maldague, X., 2004. "Pulsed phase thermography reviewed". *Quantitative InfraRed Thermography Journal*, Vol. 1, No. 1, pp. 47–70.

Ibarra-Castanedo, C. and Maldague, X., 2013. "Infrared thermography". In H. Czichos, ed., *Handbook of Technical Diagnostics*, Springer Berlin Heidelberg, pp. 175–220.

Ibarra-Castanedo, C. and Maldague, X., 2015. "Review of pulse phase thermography". In *Proc. SPIE - Thermosense: Thermal Infrared Applications XXXVII*. Vol. 9485, pp. 94850T–94850T–10.

Ibarra-Castanedo, C., Sevais, P., Ziadi, A., Klein, M. and Maldague, X., 2014. "Rita - robotized inspection by thermography and advanced processing for the inspection of aeronautical components". In *Proc. QIRT 12 âĂŞ Quantitative Infrared Thermography*. Bordeaux, France, pp. 1–8.

Maldague, X., 2001. *Theory and practice of infrared technology for nondestructive testing*. John Wiley & Sons, New York, 1st edition.

Maldague, X. and Marinetti, S., 1996. "Pulse phase thermography". *Journal of Applied Physics*, Vol. 79, No. 5, pp. 2694–2698.

Meola, C. and Carlomagno, G.M., 2004. "Recent advances in the use of infrared thermography". *Measurement science and technology*, Vol. 15, No. 9, pp. 27–58.

Meola, C., Carlomagno, G.M. and Giorleo, L., 2004. "The use of infrared thermography for materials characterization". *Journal of materials processing Technology*, Vol. 155, pp. 1132–1137.

Mian, A., Newaz, G., Han, X., Mahmood, T. and Saha, C., 2004. "Response of sub-surface fatigue damage under sonic load a computational study". *Composites Science and Technology*, Vol. 64, No. 9, pp. 1115–1122.

Oswald-Tranta, B. and Shepard, S., 2013. "Comparison of pulse phase and thermographic signal reconstruction processing methods". In *Proc. SPIE, Thermosense XXXV*. Vol. 8705, pp. 87050S1–9.

Rajic, N., 2002. "Principal component thermography for flaw contrast enhancement and flaw depth characterisation in composite structures". *Composite Structures*, Vol. 58, No. 4, pp. 521–528.

Renshaw, J., Chen, J.C., Holland, S.D. and Thompson, R.B., 2011. "The sources of heat generation in vibrothermography". *NDT & E International*, Vol. 44, No. 8, pp. 736–739.

Rothenfusser, M.J. and Homma, C., 2005. "Acoustic thermography: vibrational modes of cracks and the mechanism of heat generation". In *AIP Conference Proceedings*. Vol. 760, pp. 624–631.

Shepard, S., Ahmed, T. and Lhota, J.R., 2004. "Experimental considerations in vibrothermography". In *Proc. SPIE, Thermosense XXVID*. Vol. 5405, pp. 332–335.

Shepard, S.M., 2001. "Advances in pulsed thermography". In *Proc. SPIE, Thermosense: Thermal Infrared Applications XXVIII*. Vol. 4360, pp. 511–515.

Shepard, S.M. and Beemer, M.F., 2015. "Advances in thermographic signal reconstruction". In *Proc. SPIE - Thermosense: Thermal Infrared Applications XXXVII*. Vol. 9485, pp. 94850R–94850R–7.

Woolard, D.F. and Cramer, K.E., 2005. "Line scan versus flash thermography: Comparative study on reinforced carbon-carbon". In *Proc. SPIE, Thermosense XXVII*. Vol. 2782, pp. 315–323.

## 7. RESPONSIBILITY NOTICE

The authors are the only responsible for the printed material included in this paper.